Global modeling of brown carbon: impact of temperature- and humidity-dependent bleaching

Xinchun Xie^{1,2,3}, Yuzhong Zhang^{2,3}, Ruosi Liang^{1,2,3}, and Xuan Wang⁴

¹College of Environmental and Resource Sciences, Zhejiang University, Hangzhou, Zhejiang 310058, China ²Key Laboratory of Coastal Environment and Resources of Zhejiang Province, School of Engineering, Westlake University, Hangzhou, Zhejiang 310030, China

³Institute of Advanced Technology, Westlake Institute for Advanced Study, Hangzhou, Zhejiang 310024, China ⁴School of Energy and Environment, City University of Hong Kong,

Hong Kong SAR, China

Correspondence: Yuzhong Zhang (zhangyuzhong@westlake.edu.cn)

Received: 16 May 2025 - Discussion started: 28 May 2025 Revised: 13 August 2025 - Accepted: 15 August 2025 - Published:

Abstract. Brown carbon (BrC), a light-absorbing component of organic aerosols, undergoes bleaching in the atmosphere, a process where its light absorption capacity diminishes over time due to chemical transformation. A recent study suggests that the lifetime of freshly emitted, unbleached BrC (referred to as fresh BrC) against bleaching (τ_{BrC}) is influenced by ambient temperature and relative humidity. In this study, we incorporate the improved τ_{BrC} parameterization into an atmospheric chemical transport model (GEOS-Chem) to assess its atmospheric chemical and radiative effects. Our results show that τ_{BrC} varies strongly with altitude, ranging from 1-10h in the planetary boundary layer (PBL) to over 100h in the upper troposphere, where bleaching becomes negligible. Dry regions (e.g., northern Africa and South Asia) exhibit longer surface τ_{BrC} , while humid regions (e.g., the tropics) show shorter τ_{BrC} . The updated τ_{BrC} parameterization triples the global burden of fresh BrC compared to the baseline parameterization with uniform τ_{BrC} , increasing its effective lifetime from 0.45 to 1.45 d and amplifying the direct radiative effect (DRE) of BrC by 48 % (from +0.059 to +0.088 W m⁻²). Lofted wildfire emissions experience prolonged τ_{BrC} due to reduced bleaching in the free troposphere, underscoring the importance of fire injection height. Additionally, BrC absorption suppresses photochemical activity, reducing the photolysis rate of NO₂ (JNO₂) by up to 7.4 %, surface ozone by 0 %-2.5 %, and tropospheric OH by 0 %-6.9 %. These effects intensify during major wildfire events, such as the Siberian fires in 2019 that caused JNO₂ and ozone to drop by 36.3 % and 17.5 %, respectively, highlighting BrC's role in perturbing atmospheric oxidation capacity.

Introduction

Brown carbon (BrC), a highly complex and dynamic mixture of organic aerosols (Lin et al., 2017), can absorb sunlight in the ultraviolet (UV) and visible wavelengths, contributing to 5 the warming of the atmosphere (Washenfelder et al., 2015; Andreae and Gelencsér, 2006; Laskin et al., 2015). Previous studies indicate that BrC accounts for 7 %-19 % of total aerosol light absorption (Feng et al., 2013), with its influence reaching up to 40 %-50 % at 300-400 nm wavelengths (Lack and Langridge, 2013). Studies have reported that the atmospheric radiative forcing due to BrC can be as much as 40 % of that caused by black carbon (BC) in regions with intensive agricultural fires (Srinivas et al., 2016) and approximately 24% in the free troposphere affected by biomass burning (Zhang et al., 2017).

Biomass burning emissions are the primary source of global BrC (Andreae and Merlet, 2001; Andreae and Gelencsér, 2006), contributing $\sim 60\%$ of the BrC warming effect (Yue et al., 2022), followed by contributions from biofuel burning (e.g., residential wood combustion) (Saleh et al., 2014). Frequent and intensive wildfire events, driven by climate change, land use change, and natural variability (Fu et al., 2013; Jolly et al., 2015), have raised the concerns regarding positive feedback through wildfires (Zheng et al., 2023; Cunningham et al., 2024). Large-scale fires emit substantial amounts of aerosols, disrupting the Earth's radiation balance (Huang et al., 2023) and adversely affecting human health (Nie et al., 2018). Intensified fire activity has slowed down or even reversed the downward trend in global and regional PM_{2.5} levels (Li et al., 2023; Burke et al., 2023).

Most climate models treat BC as the only significant lightabsorbing aerosol, neglecting the contribution of BrC in the near-UV to visible range (Kelesidis et al., 2022). However, 15 recent studies have highlighted the contribution of BrC to atmospheric radiative forcing. Collow et al. (2024) found that including BrC significantly improved simulated absorption in the ultraviolet band. Zhang et al. (2020) estimated that the direct forcing effect (DRE) from BrC is around $+0.1 \,\mathrm{W}\,\mathrm{m}^{-2}$, $_{20}$ corresponding to about 25 % of the BC (0.39 W m⁻²). Feng et al. (2013) demonstrated that the radiative effect of organic aerosols in certain regions of the tropopause could shift from cooling $(-0.08 \,\mathrm{W\,m^{-2}})$ to warming $(+0.025 \,\mathrm{W\,m^{-2}})$ when BrC is included in radiative simulations, a result con-25 sistent with the findings of DeLessio et al. (2024), who reported a BrC DRE of 0.04 W m⁻². Srinivas et al. (2016) found that BrC accounts for 40 % of the atmospheric radiative forcing caused by BC, and Chung et al. (2012) estimated that 20 % of the solar radiation absorption by carbonaceous 30 aerosols at 550 nm originates from BrC. When BrC bleaching is considered, the reported global DRE values are reduced to $0.06 \,\mathrm{W}\,\mathrm{m}^{-2}$ (Brown et al., 2018) and $0.029 \,\mathrm{W}\,\mathrm{m}^{-2}$ (Drugé et al., 2022). This warming effect of carbonaceous aerosols in the troposphere is especially evident in regions 35 with significant biomass burning.

BrC primarily absorbs light in the near-UV-visible spectrum, reducing sunlight availability for photolysis reactions. This absorption alters the local photochemical environment, reducing the photolysis of nitrogen dioxide (NO2) to ni-40 tric oxide (NO) – a crucial step in ozone formation, leading to lower ozone levels in regions with high BrC concentrations. Other free radicals (e.g., OH and HO₂) are similarly affected (Wu et al., 2019). OH radicals, which are key atmospheric oxidants, are primarily generated through the re-45 action between O(1D) (produced by UV-induced ozone decomposition) and water molecules. Studies have shown that BrC emissions from biomass burning can reduce OH concentrations by 5 %-30 % in affected areas (Hammer et al., 2016). While the effects of BrC on atmospheric oxidation 50 are currently underexplored (Selimovic et al., 2020), further investigation is essential to understand their chemical implications.

Atmospheric BrC evolves through photochemical aging, where exposure to sunlight and atmospheric oxidants modi-55 fies its chemical structure and optical properties. Over short timescales, BrC can darken near its source, while bleaching and oxidative whitening occur over longer timescales (e.g., 1 d or more after emission). The bleaching time (referred to as lifetime in this study) of BrC is a critical factor that influences its climatic impact, but it remains challenging to 60 quantify accurately. Accurately parameterizing the lifetime of BrC in climate models is essential for predicting its distribution, concentration, and radiative effects. Most studies simplify BrC's lifetime to either exclude bleaching or assume a constant value of about 1 d (Feng et al., 2013; Jo et 65 al., 2016; Wang et al., 2018). However, wildfire-driven convective vertical transport can extend BrC's lifetime as particle viscosity affects its atmospheric persistence (Schnitzler et al., 2022; Xu et al., 2024). The lifetime in the upper troposphere is significantly longer than 1 d, and there are also 70 differences in different dimensional bands (Schnitzler et al., 2022). Neglecting these variations leads to inaccurate estimates of BrC's effects in models.

In this study, we update the bleaching lifetime parameterization of BrC in the GEOS-Chem atmospheric chemi- 75 cal transport model and examine the impacts of this update on the radiative effects of wildfire-derived BrC. Unlike BC, whose climate impacts are relatively well understood, BrC's atmospheric warming effect remains highly uncertain and poorly represented in climate models. Given the expected 80 increase in wildfire activity globally, quantifying BrC's radiative impacts is becoming increasingly critical. This study investigates the influence of wildfire emissions on the distribution of atmospheric BrC and systematically evaluates its climate and chemical impacts. We first update the parameterization of BrC's chemical lifetime against bleaching and examine its environmental dependence (Sect. 3.1). We then explore the global distribution of BrC (Sect. 3.2) and evaluate the simulation results against multiple ground-based and aircraft observations (Sect. 3.3). Finally, we quantify the direct 90 radiative effect (DRE) of BrC at regional and global scales (Sect. 3.4) and assess its influences on atmospheric oxidation capacity and chemical processes (Sect. 3.5).

2 Method

2.1 GEOS-Chem simulation

The global simulations utilize version 12.8 of GEOS-Chem, with a horizontal resolution of 4° × 5° and 47 vertical levels, driven by meteorology fields from the Modern Era Retrospective-analysis for Research and Applications, version 2 (MERRA-2) (Gelaro et al., 2017) 100 (https://gmao.gsfc.nasa.gov/reanalysis/MERRA-2/, last access: 20 February 2024). Global anthropogenic emissions are from EDGARv43 (Crippa et al., 2018), with region-specific updates, including APEI for Canada (Canada's Air Pollutant Emissions Inventory, 2016), NEI (2014) for the USA, 105 MIX for Asia (Li et al., 2017), and DICE_Africa for Africa (Marais and Wiedinmyer, 2016). Biofuel emissions are from

Bond et al. (2007), and daily resolved biomass burning emissions are from the Global Fire Emissions Database with small fires (GFED4s) (Giglio et al., 2013; van der Werf et al., 2017; Randerson et al., 2017). These emission inventories yield global organic carbon (OC) emissions of 42.74 Tg and BC emissions of 8.24 Tg in 2019. Of the total OC emissions, 21.17 Tg is from biomass burning, and 6.29 Tg is from biofuel burning. In the simulation, these sources are treated as BrC (see Sect. 2.2 for details), while the remaining OC emissions are modeled as purely scattering aerosols.

In the simulation, 80 % of BC, 50 % of anthropogenic OC, and 50 % of biomass burning OC is emitted as hydrophobic. These hydrophobic aerosols are converted into hydrophilic forms, which are subject to wet removal, with an e-folding 15 timescale of 1.2 d (Park and Jacobb, 2003). BC and organic aerosol (OA) are treated as externally mixed, as described in Wang et al. (2014), with absorption enhancements of 1.1 for fossil BC and 1.5 for biofuel and biomass burning BC. Primary organic aerosol (POA) is diagnosed from simulated 20 primary OC using an OA/OC mass ratio of 2.1 (Wang et al., 2018). Secondary organic aerosols (SOAs) are simulated using the simple scheme (Kim et al., 2015; Pye et al., 2010), with all SOAs being assumed to be hydrophilic. Inorganic sulfate-nitrate-ammonium aerosols are simulated fol-25 lowing Shah et al. (2020) and Shao et al. (2019), with thermodynamic equilibrium computed using the ISORROPIA II (Fountoukis and Nenes, 2007). Dust and sea salt aerosols are simulated according to Duncan Fairlie et al. (2007) and Jaeglé et al. (2011), respectively.

To evaluate the radiative impact of BrC, we use the Rapid Radiative Transfer Model for Global Circulation Models (RRTMG), coupled with GEOS-Chem, to calculate both longwave and shortwave radiative fluxes and heating rates in the atmosphere. RRTMG is invoked every 3 h, and the computation of instantaneous atmospheric radiative fluxes is performed at 30 wavelengths between 0.23 to 56 μm in the clear sky (Heald et al., 2014).

2.2 Brown carbon simulation

Our simulation treats organic aerosols from biomass or bio⁴⁰ fuel burning as light-absorbing BrC and those from fossil
fuel combustion as purely scattering. Although a few field
studies, particularly in China, have reported weak light absorption by primary organic aerosols from fossil fuel sources
(Yan et al., 2017; Chen et al., 2020), their overall contribu⁴⁵ tion is minor on the global scale and thus is not considered in
our simulation.

To capture the change in mass absorption efficiency (MAE) due to chemical processing, organic aerosols from biomass and biofuel burning are modeled as two distinct species, namely fresh BrC, which is strongly absorbing, and bleached BrC, which is weakly absorbing, following the approach by Wang et al. (2018). All freshly emitted OAs from biomass and biofuel burning are specified as fresh BrC. They

are subsequently converted into bleached BrC in the atmosphere, with the rate being governed by bleaching lifetime $\tau_{\rm BrC}$.

The BrC optical properties are implemented following Wang et al. (2018). The mean absolute errors (MAEs) of fresh BrC at different wavelengths are estimated based on the Mie theory as a function of aerosol size, aerosol density, and the refractive index. The size of OA is assumed to follow a log-normal distribution, with a geometric median diameter of 180 nm and a standard deviation of 1.6 (Wang et al., 2018). The density of OA is set at 1.3 g cm⁻³. The real part of the refractive index is 1.5, while the imaginary part and its wavelength dependence are parameterized based on the mass emission ratios of BC/OA (June et al., 2020). The BC/OA ratios are specified as 0.05 for biomass burning and 0.12 for biofuel, representing average global burning conditions (Wang et al., 2018).

Based on these parameters, Mie calculations yield an MAE of $1.3~{\rm m}^2~{\rm g}^{-1}$ at the 365 nm wavelength for fresh BrC from biomass burning and $1.2~{\rm m}^2~{\rm g}^{-1}$ for biofuel burning, with corresponding absorption Ångström exponents (AAEs) between 300 and 600 nm of 3.1 and 2.6, respectively. To account for weakened absorption by bleaching, we assume that bleached BrC absorbs only one-quarter as much as fresh BrC, resulting in MAEs of 0.37 [151] and $0.30~{\rm m}^2~{\rm g}^{-1}$ for biomass and biofuel burning aerosols, respectively, at 365 nm.

The conversion from fresh to bleached BrC is governed by the chemical lifetime τ_{BrC} (referred to as bleaching lifetime hereafter). Wang et al. (2018) parameterized this parameter as inversely proportional to the ambient hydroxyl radical (OH) concentration, specifying τ_{BrC} as $\frac{5\times 10^5}{[OH]}$ d, where [OH] is the OH concentration in molec. cm⁻³. This formulation, mainly based on empirical evidence from field measurements in the lower troposphere (Forrister et al., 2015; Wang et al., 2018), yields a τ_{BrC} of roughly 1 d throughout the troposphere.

More recent laboratory experiments by Schnitzler et 90 al. (2022) found that the chemical lifetime of water-soluble BrC, generated from smoldering pine wood in the presence of ozone, increases substantially with enhanced particle viscosity when temperature and RH get lower. Although the experimental setup (i.e., using ozone as the oxidant, generating aerosols from pine wood, and focusing on water-soluble BrC) does not fully represent atmospheric conditions, the finding that τ_{BrC} is highly sensitive to environmental parameters has critical implications for BrC's radiative and chemical effects.

To quantitatively evaluate these implications, we implement the parameterization of τ_{BrC} (in s) developed by Schnitzler et al. (2022) in GEOS-Chem. As shown in Eq. (1), τ_{BrC} depends on ambient temperature (T) and relative humidity

(RH):

$$\tau_{\rm BrC} = A \left[D_0(T) \left(\frac{\eta_0(T)}{\eta_{\rm BrC}(T, \text{RH})} \right)^{\xi} \right]^{-\frac{1}{2}},$$
(1)

where D_0 is the diffusion rate of ozone in pure water, calculated with the Stokes–Einstein equation as a function of T. η_0 is the viscosity of pure water as a function of T, and $\eta_{\rm BrC}$ is the viscosity of aqueous BrC aerosols, parameterized as a function of T and RH based on the experimental measurements (Schnitzler et al., 2022). A and ξ are treated as constants, where $A=0.125\,{\rm m\,s^{-1/2}}$ and $\xi=0.684$. $\tau_{\rm BrC}$ is calculated and updated online in the GEOS-Chem simulation, driven by T and RH data from MERRA-2.

2.3 Observation data

We use observations from aircraft campaigns (ATom mission, Fig. S1 in the Supplement) and a ground-based remote 15 sensing network (AERONET) to evaluate our simulations of BrC. The Atmospheric Tomography Mission (ATom) is a NASA-led aircraft campaign aimed at measuring and understanding the global distribution of greenhouse gases and reactive gases and aerosols (Thompson et al., 2022). The 20 ATom flights, conducted between 2016 and 2018, sampled extensive latitudinal and longitudinal ranges, from the Arctic to the Antarctic and over both the Pacific and Atlantic oceans (Prather et al., 2017). During the ATom-2, ATom-3, and ATom-4, BrC was sampled at altitudes ranging from 0.2 25 to 12 km aboard the NASA DC-8 aircraft, alongside comprehensive measurements of various gases and aerosols. Watersoluble BrC (WS BrC) in aerosols was measured with two systems: a spray chamber (MC) coupled to a liquid waveguide capillary cell (LWCC) and a particle-into-liquid sam-30 pler (NOAA PILS-LWCC) coupled to an LWCC (Washenfelder et al., 2015). The MC-LWCC system collects aerosols through a spray chamber, trapping the particles in water; these are then analyzed using an LWCC and a spectrometer. The PILS-LWCC system collects aerosols in a liquid 35 stream for similar analysis. The detection limits at 365 nm were $1.53 \,\mathrm{Mm^{-1}}$ (MC), $0.89 \,\mathrm{Mm^{-1}}$ (CSU), and $0.03 \,\mathrm{Mm^{-1}}$ (NOAA), respectively. A factor of 2 is used to convert the light absorption of BrC in the solution into the light absorption of atmospheric particles (Liu et al., 2013; Zhang 40 et al., 2017). In this study, we evaluate our simulations against the measurements taken during the ATom-4, which occurred from 24 April to 21 May 2018 (https://espoarchive. nasa.gov/archive/browse/atom/id14/DC8, last access: 25 October 2024). Samples were collected every 5 min at altitudes 45 below 3 km and every 15 min at higher altitudes, yielding a total of 1074 samples. The flight path of the ATom-4 is shown in Fig. S1.

The AERONET (AErosol RObotic NETwork) program is a federation of ground-based remote sensing aerosol net-50 works established by NASA and LOA-PHOTONS (CNRS) (Holben et al., 2006). The program provides a long-term, continuous, and readily accessible public domain database of aerosol optical, microphysical, and radiative properties. AERONET's aerosol optical depth (AOD) observations are derived from direct solar radiation in multiple wavelength 55 bands, mainly ranging from 340 to 1640 nm, while other aerosol properties (including single-scattering albedo or SSA and absorbing aerosol optical depth or AAOD) are derived from diffuse sky radiation at four wavelengths: 440, 675, 870, and 1020 nm (Dubovik and King, 2000). This study extracted AOD and AAOD at 440 nm from AERONET data in 2019 to compare with the model simulation results. We use high-quality level-2.0 AOD data (uncertainties of 0.01 in the visible range and 0.02 in the ultraviolet range) (Giles et al., 2019) and almucantar inversion AAOD data. To ensure the 65 consistency in the comparison between model simulations and observations, we sample the simulation on days and at locations when and where AOD and AAOD measurements are available.

2.4 Simulation experiments

We perform a series of global 4° × 5° GEOS-Chem simulations for 2019 to examine the impact of environmentalcondition-dependent BrC chemical lifetime (τ_{BrC}) on the abundance and distribution of BrC globally (Table 1). The baseline simulations (Base and BaFt) use the Wang 75 et al. (2018) τ_{BrC} parameterization (bleaching lifetime of roughly 1 d, largely invariant with environmental conditions). The updated simulations (Upd and UpdFt) incorporate the Schnitzler et al. (2022) τ_{BrC} parameterization as a function of temperature and RH (Eq. 1). To test the impact of the vertical partitioning of fire emissions and its interactions with τ_{BrC} parameterizations, we perform GEOS-Chem simulations that assign 100 % (0 %) (Base and Upd) and 65 % (35 %) (BaFt and UpdFt) of wildfire emissions (all fire-emitted species including BC and BrC) in the boundary layer (free troposphere). The 65%:35% partitioning is based on the averages of aerosol smoke plume heights observed by the Multi-angle Imaging SpectroRadiometer (MISR) (Val Martin et al., 2010) and has been previously applied in GEOS-Chem modeling studies to assess the impact of fire plume heights (Fischer et 90 al., 2014; Jin et al., 2023). In addition to 2019, we also run the April and May 2018 simulation to evaluate against the ATom-4 observations. We also use the GFED5 beta version to test the sensitivity to biomass emission inventories.

3 Results and discussion

3.1 Chemical lifetime of BrC against bleaching

Figure 1 shows the spatial distribution of τ_{BrC} as parameterized based on Schnitzler et al. (2022). In the planetary boundary layer (< 1.5 km), τ_{BrC} is roughly 1–10 h, indicating that BrC's light-absorbing capacity rapidly degrades on

Table 1. Descriptions of model sensitivity experiments.

Experiments	Lifetime	Emission inventory	Fire emission fraction under PBL
Base BaFt Upd UpdFt UpdGF5	Original τ_{BrC} Original τ_{BrC} Updated τ_{BrC} Updated τ_{BrC} Updated τ_{BrC}	GFED4s GFED4s GFED4s GFED5	100 % 65 % 100 % 65 % 100 %

the timescale of 1 d, generally consistent with ground or lower-troposphere observations (Laskin et al., 2015; Forrister et al., 2015). τ_{BrC} increases dramatically with altitude, driven primarily by decreased temperature. τ_{BrC} reaches $10^{2.5}$ h after ≈ 2 weeks in the mid-troposphere at ~ 4 km, comparable to the lifetime of aerosols against wet and dry deposition. At higher altitudes, τ_{BrC} increases further by several orders of magnitude, rendering photo-bleaching effectively negligible in the upper troposphere, which is supported by a few analyses of high-altitude measurements (Liu et al., 2014; Zhang et al., 2017).

In addition to vertical variations, τ_{BrC} also varies considerably across different regions of the globe (Fig. S2a). The horizontal variations at the same altitude appear to be controlled mainly by relative humidity (Fig. S2). At the surface and in the lower troposphere, τ_{BrC} tends to be several days longer in dry regions such as northern Africa, Middle Asia, the western US, northern Australia, southern Africa, and southern America. In the free troposphere, τ_{BrC} is shorter in the Intertropical Convergence Zone because of the higher humidity due to convective updrafts.

In contrast, the [OH]-dependent parameterization of τ_{BrC} implemented in Wang et al. (2018) exhibits much smaller spatial variations, predicting τ_{BrC} to be on the order of 1 d throughout the troposphere. The [OH]-dependent parameterization was constructed based on very few field studies, mostly in lower-troposphere conditions (Forrister et al., 2015). The two parameterizations predict similar τ_{BrC} in the planetary boundary layer but differ greatly in the middle and upper troposphere. These differences would have important implications for the global distribution and the radiative impact of primary organic aerosols from biomass and biofuel burning.

3.2 Global distribution of fresh BrC

Figure 2a shows the global distribution of fresh BrC column density in 2019, which reveals elevated concentrations in regions characterized by substantial biomass burning and biofuel emissions (Fig. S3). These hotspots include tropical Africa (biomass), tropical South America (biomass),
 East Siberia (biomass), South Asia (biofuel), and East China (biofuel). Compared to the baseline simulation (BaFt), the updated simulation (UpdFt) with temperature- and RH-

dependent τ_{BrC} yields higher fresh BrC concentrations across most regions. The largest increase is observed in southern Africa, which is due to long τ_{BrC} near the surface (Fig. 1) resulting from the region's strong biomass burning emissions (Fig. S3) and dry environmental conditions (Fig. S2). Conversely, despite intensive wildfire emissions in East Siberia, the updated simulation shows minimal differences in terms of fresh BrC concentrations because of comparable τ_{BrC} values between the two parameterizations (Fig. S2a).

Figure 3 compares the vertical profiles and average column densities of fresh BrC concentrations across simulations. The updated simulation (UpdFt), with revised τ_{BrC} and fire injection parameterizations, yields the highest fresh BrC 55 concentrations, with average column densities of 235 µg m⁻² in the tropics, $172 \,\mu\mathrm{g}\,\mathrm{m}^{-2}$ in the northern extratropics, and $24 \,\mu \mathrm{g} \,\mathrm{m}^{-2}$ in the southern extratropics. These values represent increases of factors of 4.7, 1.6, and 8.6, respectively, compared to the base simulation. Globally, the updated simulation (UpdFt) produces an average column density of $144.4 \,\mu\mathrm{g}\,\mathrm{m}^{-2}$, about 3 times that of the baseline simulation (base, $53.0 \,\mu \mathrm{g} \,\mathrm{m}^{-2}$). Given the global average emission fluxes of BrC, this result translates into an effective τ_{BrC} of 1.45 d in the UpdFt simulation as compared to 0.45 d in the base simulation. Comparison with BaFt and Upd simulations (average column density of 52.9 and 120.7 μ g m⁻²) suggests that the increase in BrC abundance in UpdFt relative to the base is mainly due to the bleaching lifetime update.

Vertical profiles of fresh BrC demonstrate significant differences between the UpdFt and base simulations. The absolute differences are particularly large in the lower troposphere of the tropics, reaching up to $0.05\,\mu g\,m^{-3}$, while relative differences are most pronounced in the upper troposphere, exceeding a factor of 10 despite lower absolute concentrations. Meanwhile, the updated τ_{BrC} parameterization does not change the total BrC concentrations (fresh + bleached BrC) (Fig. S4) as the abundance of total BrC is controlled by the rate of wet and dry deposition.

The influence of τ_{BrC} parameterization on fresh BrC concentrations is modulated by fire emission injection height. Direct injection of emissions into the free troposphere results in slower BrC bleaching and higher concentrations at elevated altitudes. Comparing results from UpdFt and Upd simulations, we find that, under environmental-conditiondependent τ_{BrC} parameterization, injecting 35 % of fire emissions into the free troposphere (UpdFt) (Thapa et al., 2022) leads to 30 %-50 % greater fresh BrC burdens compared to those with emissions confined to the surface layer (Upd) (Fig. 3). In contrast, under the original uniform τ_{BrC} , different treatments of fire emission injections (BaFt and Base) affect only the vertical distribution of BrC without influencing its overall atmospheric burden (Fig. 3). These results underscore the interactions between τ_{BrC} and fire emission injection heights.

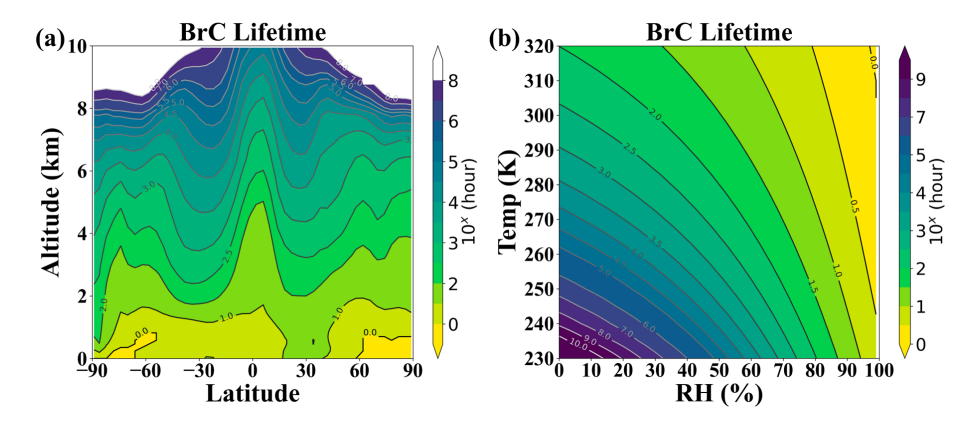


Figure 1. The lifetime of BrC as a function of altitude and latitude (a) and as a function of temperature and relative humidity (b).

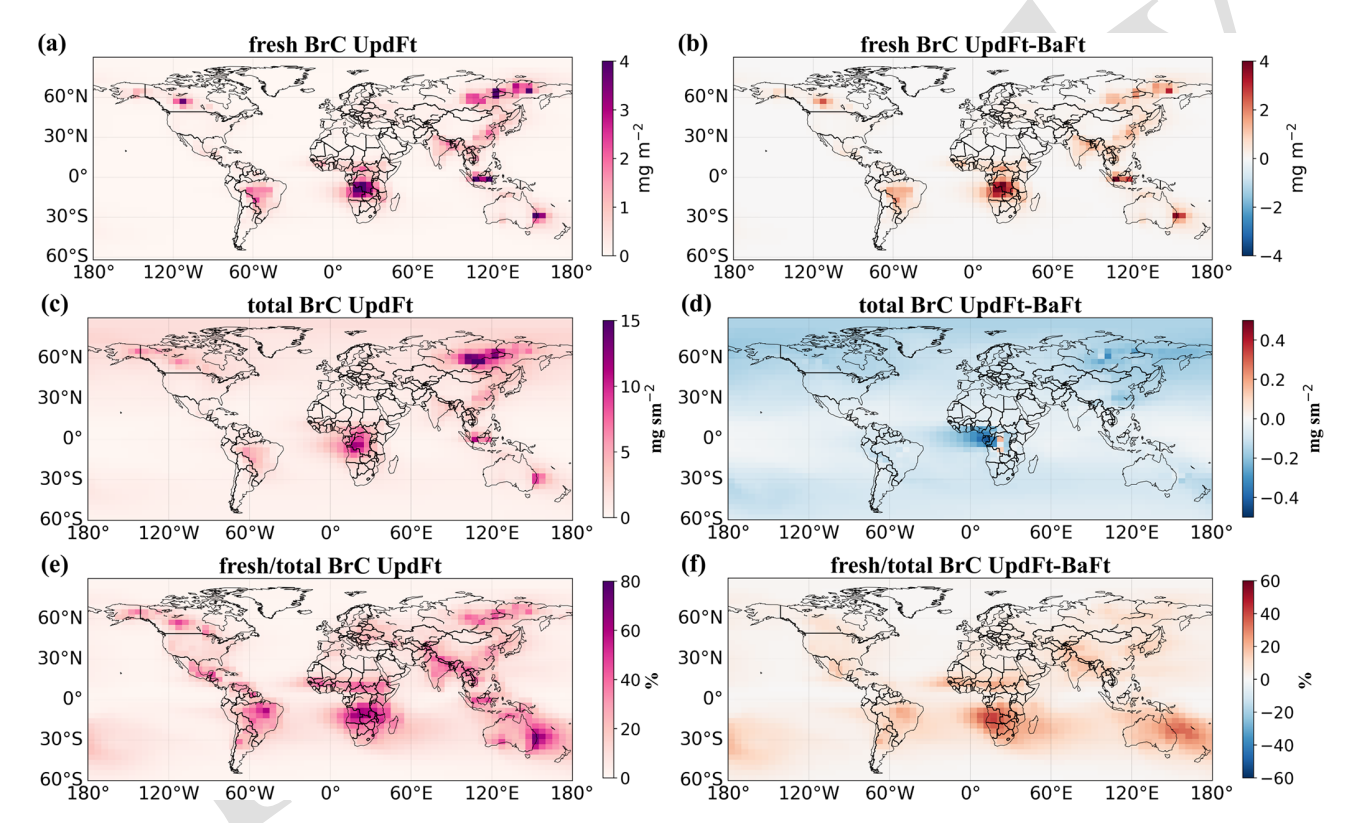


Figure 2. Global distribution of fresh BrC column density (a), total BrC (fresh BrC + bleached BrC) column density (c), and the ratio of fresh to total BrC (e) with updated τ_{BrC} (UpdFt). Difference in terms of the global distribution of BrC column density (b), total BrC (fresh BrC + bleached BrC) column density (d), and the ratio of fresh to total BrC (f) between updated τ_{BrC} and original τ_{BrC} simulations (UpdFt and BaFt).

3.3 Evaluation against observations

We compare our simulations with the aircraft campaign of the ATom-4, which measured the global distribution of BrC over remote oceans (Fig. S1) (Zeng et al., 2020). The base- line simulation severely underestimates BrC absorption at 365 nm (Abs₃₆₅) (Fig. 4a). The updated simulation with longer τ_{BrC} increases fresh BrC concentrations and, hence, their Abs₃₆₅ by about an order of magnitude, bringing the

simulation results closer to but still lower than the observations (Fig. 4a). Meanwhile, the model generally captures observed levels of OA and CO during the ATom-4 but with an underestimation of OA in the upper troposphere and an overestimation of CO in the lower troposphere (Fig. 4).

Figures 5 and 6 show the comparison of the annual means of AOD and AAOD simulation results against the AERONET observations. The model, in general, reproduces both the magnitude and the distribution of observed AOD

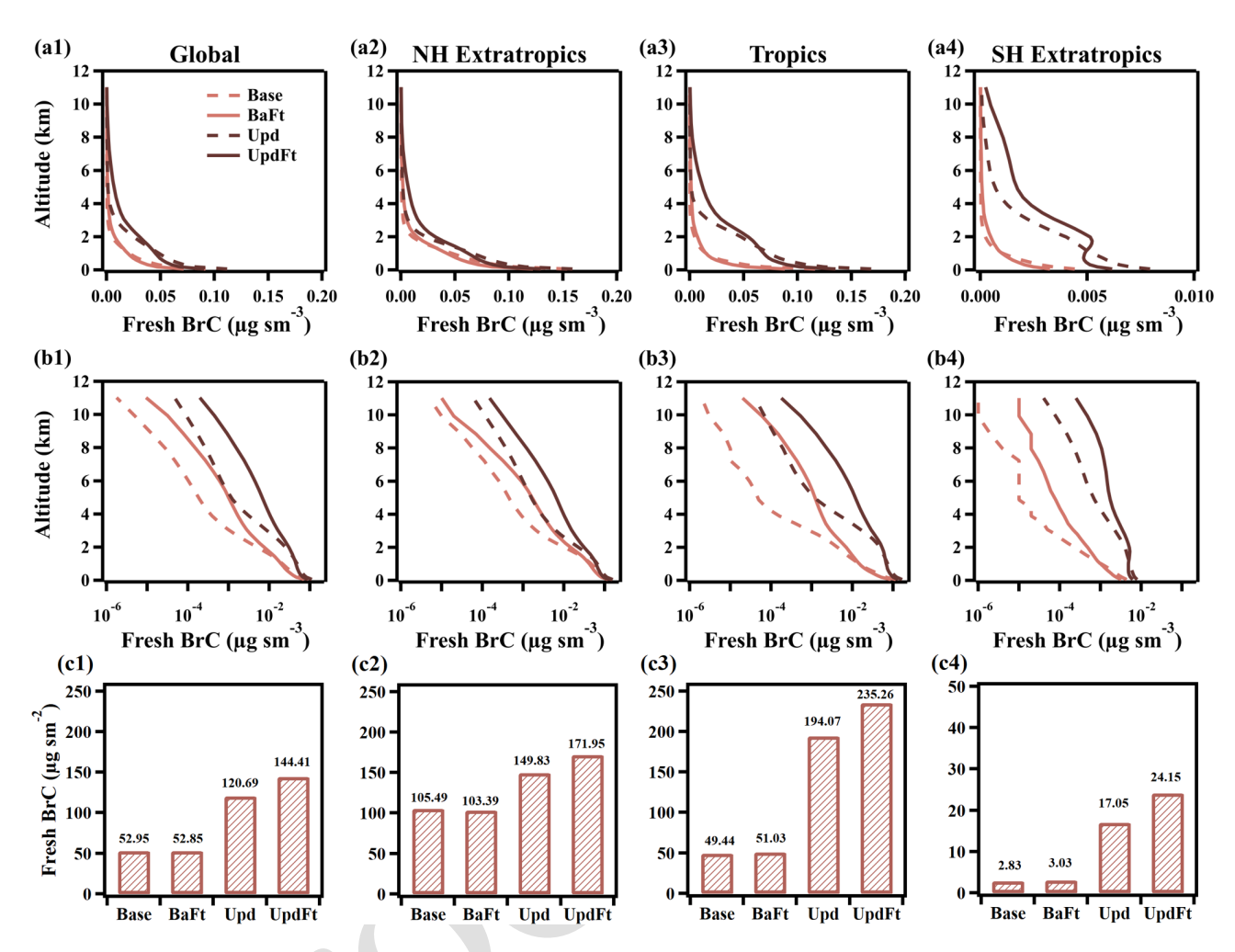


Figure 3. Vertical profiles (**a**, **b**) and column densities (**c**) of fresh BrC concentrations globally and in the Northern Hemisphere extratropics, the tropics, and the Southern Hemisphere extratropics as simulated by the GEOS-Chem model.

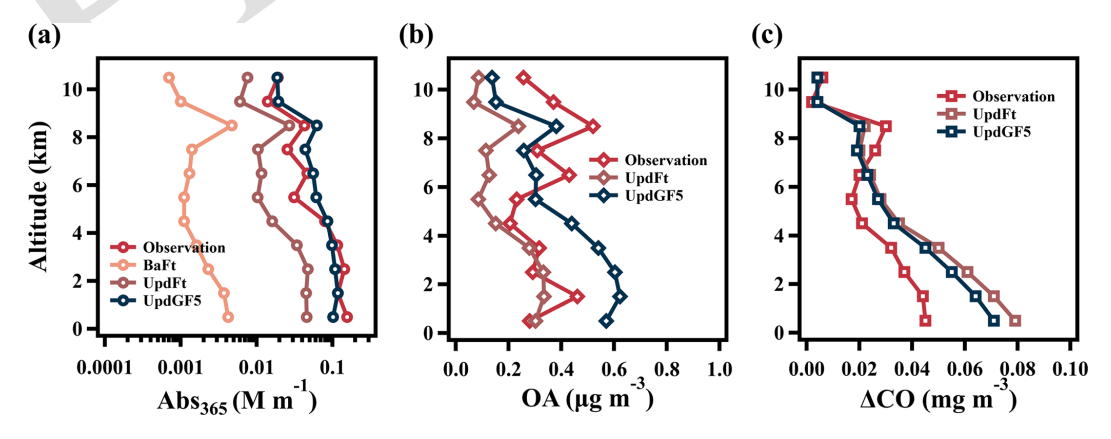


Figure 4. Vertical distribution of the median light absorption coefficient of BrC at 365 nm (a), total OA concentration (b), and Δ CO concentration (c) from simulations and observations (ATom-4). Δ CO is calculated as the CO concentration minus the background value (0.064 mg m⁻³ for observations, 0.0194 mg m⁻³ for UpdFt, and 0.0189 mg m⁻³ for UpdGF5).

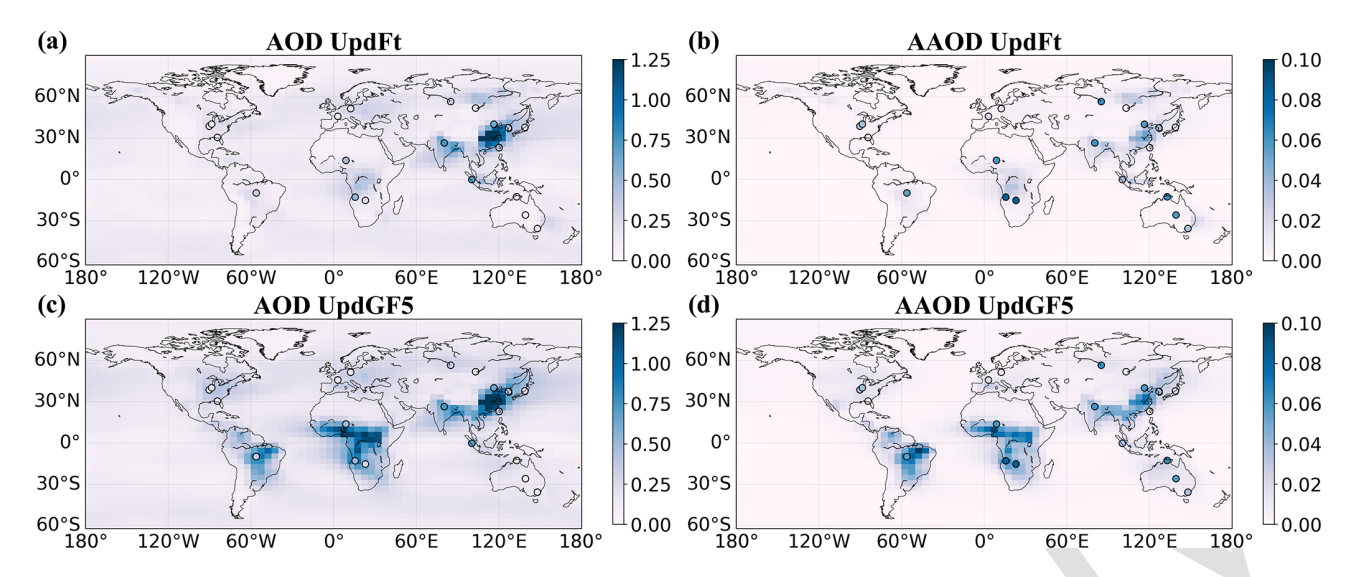


Figure 5. Global annual mean distribution of AOD (a, c) and AAOD (b, d) at 440 nm with updated τ_{BrC} using GFED4s (a, b) and GFED5 (c, d) emission inventories. The dots are the observed annual AOD and AAOD from AERONET at 440 nm.

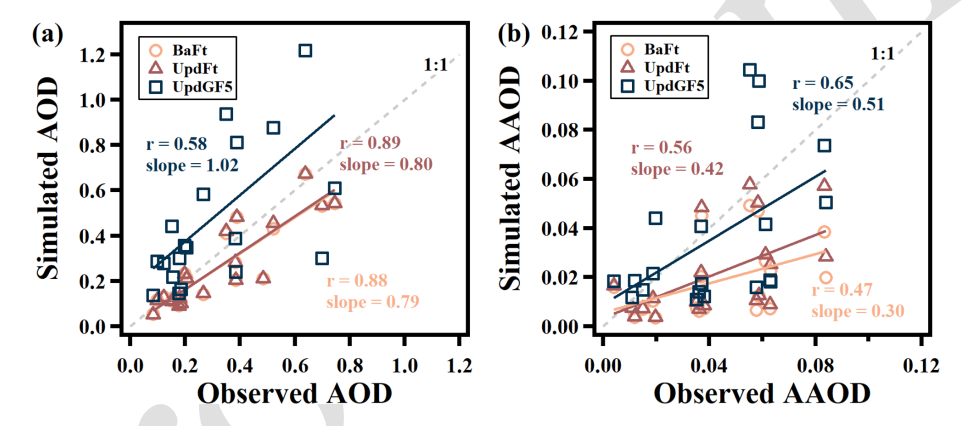


Figure 6. Comparison between observed and simulated AOD (a) and AAOD (b). Observations are from AERONET.

well. The model also captures the high AAOD observed in southern and eastern Asia, where the absorption is mainly due to BC from anthropogenic sources, but underestimates the high AAOD observed in regions with a strong influsence of biomass burning, such as Africa, South America, and Siberia (Fig. 5). Both the baseline and updated simulation show good agreement with observed AOD (R = 0.88 and slope = 0.79 in BaFt and R = 0.89 and slope = 0.80 in UpdFt). The updated UpdFt simulation (R = 0.56 and slope = 0.42) improves agreement with AAOD observations relative to the BaFt simulation (R = 0.47 and slope = 0.30) but still has notable underestimation (Fig. 6). Meanwhile, at some stations with low SSA values, the simulated SSA is overestimated (Fig. S5).

The underestimation of Abs₃₆₅ against ATom-4 data (Fig. 4) and AAOD against AERONET data (Figs. 5 and 6) may be partly explained by underestimation of biomass burning emissions. We perform additional simulations with

the newly released GFED5 fire emission inventory (https: //globalfiredata.org/, last access: 10 April 2025), which generally predicts higher biomass burning emissions than the GFED4s inventory. This simulation leads to better alignment with both ATOM-4 Abs₃₆₅ (Fig. 4) and AERONET AAOD observations (Fig. 6). However, the GFED5 simulation also leads to an overestimation of OA in the lower troposphere against ATom-4 data and of AOD against AERONET data (Figs. 4 and 6).

Additionally, there are also considerable uncertainties in the BrC simulation associated with its optical properties. The MAE values applied in different modeling studies vary considerably (Zhang et al., 2020; Jo et al., 2016), and laboratory measurements have also demonstrated source- and season-dependent differences in MAE (Chen et al., 2018; Xie et al., 2020). Moreover, assumptions about particle size distribution and refractive index also contribute to the uncertainties and need to be further constrained using observational and exper-

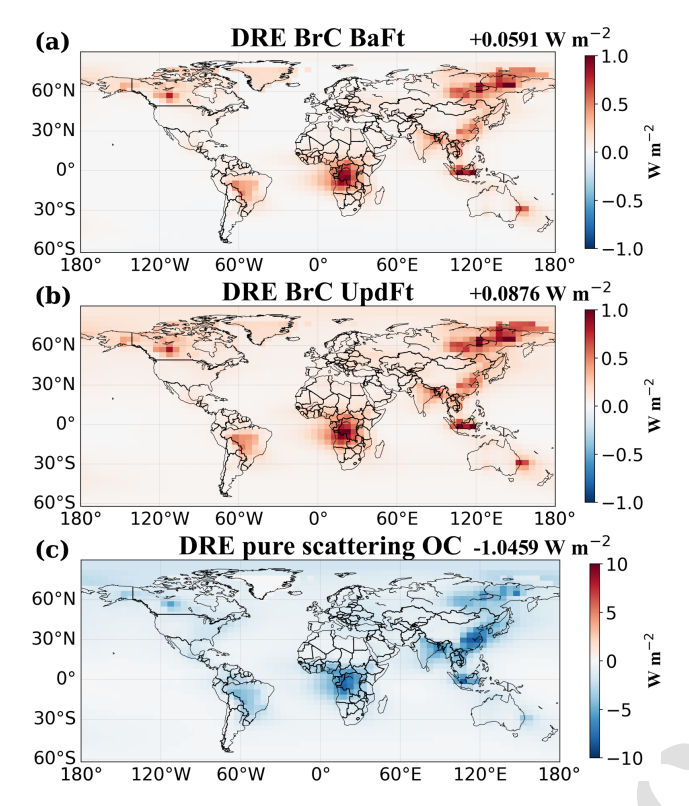


Figure 7. The DRE of original τ_{BrC} (a) and updated τ_{BrC} (b) and pure-scattering OC (c).

imental data (Wu et al., 2020; Shamjad et al., 2018). Future improvement of BrC simulations may include refined treatment of these factors.

3.4 Direct radiative effect of BrC

5 The presence of BrC enhances the overall absorptivity of aerosols, leading to positive direct radiative effects (DREs) at the top of the atmosphere. Incorporating an improved τ_{BrC} parameterization into the model increases the DRE of BrC absorption from $+0.059 \, \mathrm{W \, m^{-2}}$ in the baseline simulation to $_{10}$ +0.088 W m⁻² in the UpdFT simulation (Fig. 7). This 48 % enhancement in DRE highlights the sensitivity of BrC's radiative effects to the rate of bleaching. Our estimate of the BrC DRE is within the estimates by previous studies (0.04– $0.11 \,\mathrm{W}\,\mathrm{m}^{-2}$) (Feng et al., 2013; Zhang et al., 2020; Wang et ₁₅ al., 2018). The value is higher than the estimate by Wang et al. $(2018) (+0.048 \text{ W m}^{-2})$, which did not account for longer τ_{BrC} in the cold and dry environment, but is lower than that reported by Zhang et al. (2020) $(+0.10 \,\mathrm{W m^{-2}})$, who made an assumption that convection-lofted BrC does not photo-20 bleach. The light absorption of BrC reduces the negative DRE of OA by 5.7% in the base simulation and by 8.4% in the UpdFT simulation (Fig. 7).

3.5 Effects of BrC on atmospheric chemistry

BrC reduces the ultraviolet light available for photochemical reactions, affecting atmospheric chemistry. Figure 8 evaluates the effect of BrC light absorption on the photolysis rate of NO_2 (JNO₂) and concentrations of O_3 and OH radicals. The effects are most pronounced in regions with substantial biomass burning emissions. The annual average of JNO₂ decreases by 0%–7.4%, while surface ozone levels decline by 0%–2.5%. These results are consistent with but slightly lower than the results of Jo et al. (2016). The light absorption of BrC also results in a 0%–6.9% reduction in tropospheric OH concentration, which is also lower than the values reported for the Northern Hemisphere in Jo et al. (2016) (0%–00 and Jiang et al. (2012) (up to 15%),

The effects of BrC on atmospheric chemistry are more substantial in the season and region with intensive biomass burning. For instance, the reductions in JNO₂ and the surface ozone concentration due to BrC reached 36.3% and 4 ppb (17.5%), respectively, in high-latitude Siberia, Russia, in August 2019 (Fig. S6), when a large wildfire event occurred (Konovalov et al., 2021a, b). Another example is the large wildfire over tropical Malaysia in September 2019, which accounted for approximately 40% of the annual total wildfire emissions. In this case, JNO₂ decreased by about 27.6%, and surface O₃ concentrations decreased by as much as 6.4 ppb (10.8%) (Fig. S7).

Figure S8 shows the overall responses of atmospheric chemistry to wildfire emissions, including reactive gases and aerosols. Wildfire emissions increase tropospheric ozone concentrations across the globe while increasing OH concentrations near fire sources and suppressing OH concentrations away from the source. Comparison of Figs. S8 and 8 shows that including BrC light absorption partially offsets the ozone enhancement from wildfire emissions. Moreover, BrC absorption reduces near-source OH enhancement caused by fires while reinforcing OH reduction globally. These results demonstrate that neglecting BrC light absorption in models leads to moderate biases in simulated chemical responses to wildfire emissions.

4 Discussion

In this study, we adopt the bleaching lifetime parameterization derived from Schnitzler et al. (2022), who demonstrated that BrC bleaching rates are governed by aerosol viscosity, which itself depends strongly on temperature and relative humidity (RH). This environmental dependence introduces significant regional and vertical variability into BrC transformation, which is in marked contrast to rather uniform bleaching lifetime of $\sim 1~\mathrm{d}$ applied in previous modeling studies.

The finding by Schnitzler et al. (2022) is consistent with observations by Zhang et al. (2017), who identified a substantial presence of BrC at high altitudes over regions affected by biomass burning. An earlier modeling study (Zhang et

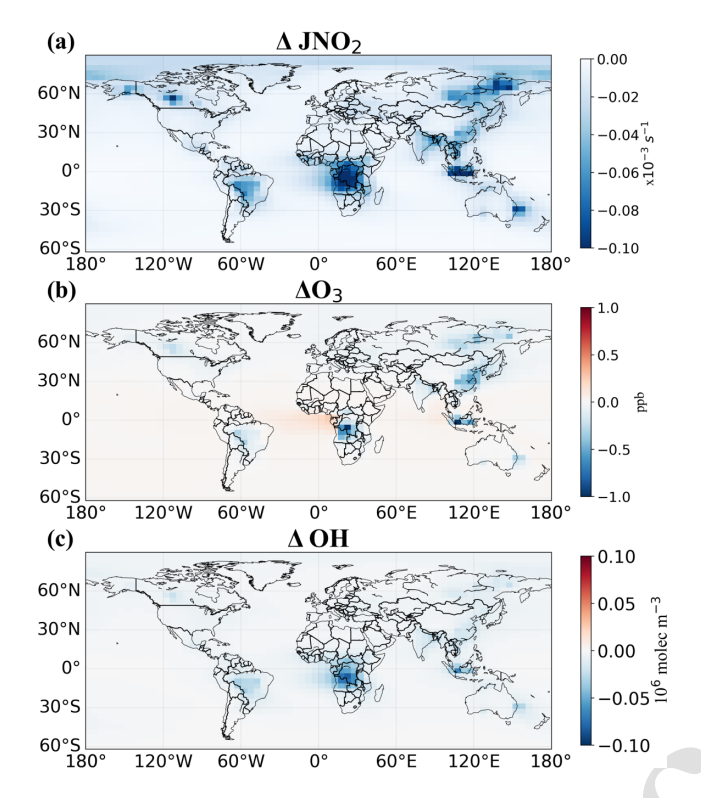


Figure 8. The effect of BrC absorption on global surface photolysis rates of JNO₂ (\mathbf{a}), O₃ (\mathbf{b}), and column OH (\mathbf{c}).

al., 2020) attempted to reconcile such observations with short bleaching lifetimes by assuming infinite lifetimes of convection-lofted aerosols, albeit without mechanistic justification. Schnitzler et al. (2022) provide this missing mechanistic basis.

While representing an important step forward, several aspects of the Schnitzler et al. (2022) parameterization merit further investigation. First, the experiment examined only ozone-driven bleaching. The role of other oxidants such as 10 OH and their sensitivity to environmental parameters are yet to be explored. Second, the study focused on water-soluble BrC, though field evidence indicates that water-insoluble BrC accounts for a large fraction of BrC absorption. The impact of temperature and RH on the bleaching behaviors of 15 water-insoluble BrC remains uncharacterized. Third, the parameterization is derived from BrC produced by smoldering pinewood, while real-world BrC properties may vary considerably across different fuel types and combustion conditions (Sun et al., 2021; Cai et al., 2023). Finally, neither the current 20 study nor Schnitzler's work addresses secondary BrC formation pathways, which may involve different bleaching mechanisms. These limitations highlight important directions for future research to further refine the representation of BrC transformation in atmospheric models.

5 Conclusions

This study implements an updated τ_{BrC} parameterization developed by Schnitzler et al. (2022) in the GEOS-Chem model and evaluates its impact on BrC's radiative and chemical effects. τ_{BrC} is parameterized to strongly depend on temperature and relative humidity. This results in τ_{BrC} that varies by orders of magnitude, from just a few hours in warm, humid boundary layers to over 2 weeks in cold, dry upper atmospheres. In contrast, the original parameterization in the model is a function of OH concentration and thus is rather uniform throughout the troposphere.

Compared to the original parameterization, the revised τ_{BrC} increases the global average BrC lifetime from 0.45 to 1.45 d, leading to a tripling of global fresh BrC burdens. The revised τ_{BrC} also leads to higher BrC concentrations in the middle and upper troposphere, particularly evident over source regions with deep convective activity, such as Central Africa and South Asia. In addition, injecting fire emissions into the free troposphere increases fresh BrC burdens by 30 %–50 % relative to surface-only emissions, highlighting the interplay between fire injection and BrC persistence.

The updated τ_{BrC} parameterization improves the agreement between simulation and observations, particularly in the upper troposphere, but still generally underestimates BrC absorption (Abs₃₆₅) in the ATom-4 campaign and AAOD in AERONET biomass burning regions. Using the GFED5 fire emission inventory, which has higher wildfire emissions, instead of GFED4s can address these underestimations but leads to overestimations in OA and AOD.

The revised bleaching lifetimes lead to a 48% increase in BrC's global direct radiative effect, from +0.059 to $+0.088\,\mathrm{W\,m^{-2}}$, compared to conventional fixed-lifetime approaches. BrC DRE surpasses BC DRE in regions with significant biomass burning, underlining its important role in the regional radiation budget and its contribution to canceling out the negative DRE of OA.

In addition, the light absorption of BrC influences atmospheric chemistry by reducing the JNO₂ rate (0%-7.4%), surface ozone concentrations (0%-2.5%), and tropospheric OH concentrations (0%-6.9%). The strongest effects were observed during intense wildfire events, with decreases of more than 36% in JNO₂ and more than 17% in ozone. In addition, BrC suppresses the enhancement of ozone and near-source OH from wildfire emissions while amplifying global-scale OH reduction due to wildfire emissions, demonstrating its role in regulating atmospheric responses to wildfires.

Code and data availability. The source code of GEOS-Chem 12.8.2 can be downloaded at https://doi.org/10.5281/zenodo.3860693 (The International GEOS-Chem User Community, 2020). The code for the updated BrC simulation is available at (last access: 15 May 2025) and 75 is archived at https://doi.org/10.5281/zenodo.17346391 (xe_xie,

2025) [152]. All data can be obtained from the corresponding author upon request.

Supplement. The supplement related to this article is available online at [the link will be implemented upon publication].

5 Author contributions. XX and YZ conceived and designed the study. XX performed the model development under the guidance of YZ and XW. XX performed all of the model simulations, data analyses, and visualizations. RL assisted with the coding. XX wrote the initial draft. YZ and XX revised the paper with contributions from all of the authors.

Competing interests. The contact author has declared that none of the authors has any competing interests.

Disclaimer. Publisher's note: Copernicus Publications remains neutral with regard to jurisdictional claims made in the text, published maps, institutional affiliations, or any other geographical representation in this paper. While Copernicus Publications makes every effort to include appropriate place names, the final responsibility lies with the authors. Views expressed in the text are those of the authors and do not necessarily reflect the views of the publisher.

- 20 Acknowledgements. The authors thank the High-Performance Computing Center of Westlake University and the National Supercomputing Center at Wuxi for the facility support and technical assistance. Xinchun Xie thanks Elijah Schnitzler for the valuable discussions, which provided important insights for this study.
- 25 Financial support. This research has been supported by the National Natural Science Foundation of China (grant no. 42275112).

Review statement. This paper was edited by Kostas Tsigaridis and reviewed by two anonymous referees.

References

- 30 Andreae, M. O. and Gelencsér, A.: Black carbon or brown carbon? The nature of light-absorbing carbonaceous aerosols, Atmos. Chem. Phys., 6, 3131–3148, https://doi.org/10.5194/acp-6-3131-2006, 2006.
- Andreae, M. O. and Merlet, P.: Emission of trace gases and aerosols from biomass burning, Global Biogeochem. Cycles, 15, 955–966, https://doi.org/10.1029/2000gb001382, 2001.
- Bond, T. C., Bhardwaj, E., Dong, R., Jogani, R., Jung, S., Roden, C., Streets, D. G., and Trautmann, N. M.: Historical emissions of black and organic carbon aerosol from energy-related
- combustion, 1850–2000, Global Biogeochem. Cycles, 21, 1–16, https://doi.org/10.1029/2006gb002840, 2007.

- Brown, H., Liu, X., Feng, Y., Jiang, Y., Wu, M., Lu, Z., Wu, C., Murphy, S., and Pokhrel, R.: Radiative effect and climate impacts of brown carbon with the Community Atmosphere Model (CAM5), Atmos. Chem. Phys., 18, 17745–17768, https://doi.org/10.5194/acp-18-17745-2018, 2018.
- Burke, M., Childs, M. L., de la Cuesta, B., Qiu, M., Li, J., Gould, C. F., Heft-Neal, S., and Wara, M.: The contribution of wildfire to PM_{2.5} trends in the USA, Nature, 622, 761–766, https://doi.org/10.1038/s41586-023-06522-6, 2023.
- Cai, J., Jiang, H., Chen, Y., Li, J., and Zhang, G.: Emission characteristics and optical properties of brown carbon during combustion of pine at different ignition temperatures under high-time resolution, Fuel, 354, 129400, https://doi.org/10.1016/j.fuel.2023.129400, 2023.
- Canada's Air Pollutant Emissions Inventory: https://Canada.ca/ APEI, last access: 27 May 2024.
- Chen, Y., Ge, X., Chen, H., Xie, X., Chen, Y., Wang, J., Ye, Z., Bao, M., Zhang, Y., and Chen, M.: Seasonal light absorption properties of water-soluble brown carbon in atmospheric fine particles in Nanjing, China, Atmos. Environ., 187, 230–240, https://doi.org/10.1016/j.atmosenv.2018.06.002, 2018.
- Chen, Y., Xie, X., Shi, Z., Li, Y., Gai, X., Wang, J., Li, H., Wu, Y., Zhao, X., Chen, M., and Ge, X.: Brown carbon in atmospheric fine particles in Yangzhou, China: Light absorption properties and source apportionment, Atmos. Res., 244, 105028, https://doi.org/10.1016/j.atmosres.2020.105028, 2020.
- Chung, C. E., Ramanathan, V., and Decremer, D.: Observationally constrained estimates of carbonaceous aerosol radiative forcing, P. Natl. Acad. Sci. USA, 109, 11624–11629, https://doi.org/10.1073/pnas.1203707109, 2012.
- Collow, A. B., Colarco, P. R., da Silva, A. M., Buchard, V., Bian, H., Chin, M., Das, S., Govindaraju, R., Kim, D., and Aquila, V.: Benchmarking GOCART-2G in the Goddard Earth Observing System (GEOS), Geosci. Model Dev., 17, 1443–1468, 75 https://doi.org/10.5194/gmd-17-1443-2024, 2024.
- Crippa, M., Guizzardi, D., Muntean, M., Schaaf, E., Dentener, F., van Aardenne, J. A., Monni, S., Doering, U., Olivier, J. G. J., Pagliari, V., and Janssens-Maenhout, G.: Gridded emissions of air pollutants for the period 1970–2012 within EDGAR v4.3.2, Earth Syst. Sci. Data, 10, 1987–2013, https://doi.org/10.5194/essd-10-1987-2018, 2018.
- Cunningham, C. X., Williamson, G. J., and Bowman, D.: Increasing frequency and intensity of the most extreme wildfires on Earth, Nat. Ecol. Evol., https://doi.org/10.1038/s41559-024-02452-2, 85 2024.
- DeLessio, M. A., Tsigaridis, K., Bauer, S. E., Chowdhary, J., and Schuster, G. L.: Modeling atmospheric brown carbon in the GISS ModelE Earth system model, Atmos. Chem. Phys., 24, 6275–6304, https://doi.org/10.5194/acp-24-6275-2024, 2024.
- Drugé, T., Nabat, P., Mallet, M., Michou, M., Rémy, S., and Dubovik, O.: Modeling radiative and climatic effects of brown carbon aerosols with the ARPEGE-Climat global climate model, Atmos. Chem. Phys., 22, 12167–12205, https://doi.org/10.5194/acp-22-12167-2022, 2022.
- Dubovik, O. and King, M. D.: A flexible inversion algorithm for retrieval of aerosol optical properties from Sun and sky radiance measurements, J. Geophys. Res.-Atmos., 105, 20673–20696, https://doi.org/10.1029/2000jd900282, 2000.

- Duncan Fairlie, T., Jacob, D. J., and Park, R. J.: The impact of transpacific transport of mineral dust in the United States, Atmos. Environ., 41, 1251–1266, https://doi.org/10.1016/j.atmosenv.2006.09.048, 2007.
- ⁵ Feng, Y., Ramanathan, V., and Kotamarthi, V. R.: Brown carbon: a significant atmospheric absorber of solar radiation?, Atmos. Chem. Phys., 13, 8607–8621, https://doi.org/10.5194/acp-13-8607-2013, 2013.
- Fischer, E. V., Jacob, D. J., Yantosca, R. M., Sulprizio, M. P., Millet, D. B., Mao, J., Paulot, F., Singh, H. B., Roiger, A., Ries, L., Talbot, R. W., Dzepina, K., and Pandey Deolal, S.: Atmospheric peroxyacetyl nitrate (PAN): a global budget and source attribution, Atmos. Chem. Phys., 14, 2679–2698, https://doi.org/10.5194/acp-14-2679-2014, 2014.
- Forrister, H., Liu, J., Scheuer, E., Dibb, J., Ziemba, L., Thornhill, K. L., Anderson, B., Diskin, G., Perring, A. E., Schwarz, J. P., Campuzano-Jost, P., Day, D. A., Palm, B. B., Jimenez, J. L., Nenes, A., and Weber, R. J.: Evolution of brown carbon in wildfire plumes, Geophys. Res. Lett., 42, 4623–4630, https://doi.org/10.1002/2015gl063897, 2015.
- Fountoukis, C. and Nenes, A.: ISORROPIA II: a computationally efficient thermodynamic equilibrium model for K⁺– Ca²⁺–Mg²⁺–NH₄⁺–Na⁺–SO₄²–NO₃⁻–Cl⁻–H₂O aerosols, Atmos. Chem. Phys., 7, 4639–4659, https://doi.org/10.5194/acp-7-4639-2007, 2007.
- Fu, X., Wang, S., Zhao, B., Xing, J., Cheng, Z., Liu, H., and Hao, J.: Emission inventory of primary pollutants and chemical speciation in 2010 for the Yangtze River Delta region, China, Atmos. Environ., 70, 39–50, https://doi.org/10.1016/j.atmosenv.2012.12.034, 2013.
- Gelaro, R., McCarty, W., Suarez, M. J., Todling, R., Molod, A., Takacs, L., Randles, C., Darmenov, A., Bosilovich, M. G., Reichle, R., Wargan, K., Coy, L., Cullather, R., Draper, C., Akella, S., Buchard, V., Conaty, A., da Silva, A., Gu, W., Kim, G. K.,
- Koster, R., Lucchesi, R., Merkova, D., Nielsen, J. E., Partyka, G., Pawson, S., Putman, W., Rienecker, M., Schubert, S. D., Sienkiewicz, M., and Zhao, B.: The Modern-Era Retrospective Analysis for Research and Applications, Version 2 (MERRA-2), J. Climate, 30, 5419–5454, https://doi.org/10.1175/JCLI-D-16-0758.1, 2017.
- Giglio, L., Randerson, J. T., and van der Werf, G. R.: Analysis of daily, monthly, and annual burned area using the fourthgeneration global fire emissions database (GFED4), J. Geophys. Res.-Biogeo., 118, 317–328, https://doi.org/10.1002/jgrg.20042, 2013
- Giles, D. M., Sinyuk, A., Sorokin, M. G., Schafer, J. S., Smirnov, A., Slutsker, I., Eck, T. F., Holben, B. N., Lewis, J. R., Campbell, J. R., Welton, E. J., Korkin, S. V., and Lyapustin, A. I.: Advancements in the Aerosol Robotic Network (AERONET) Version 3 database automated near-real-time quality control algorithm with improved cloud screening for Sun photometer aerosol optical depth (AOD) measurements, Atmos. Meas. Tech., 12, 169–
- 209, https://doi.org/10.5194/amt-12-169-2019, 2019.

 Hammer, M. S., Martin, R. V., van Donkelaar, A., Buchard, V.,
 Torres, O., Ridley, D. A., and Spurr, R. J. D.: Interpreting the
 ultraviolet aerosol index observed with the OMI satellite instrument to understand absorption by organic aerosols: implications for atmospheric oxidation and direct radiative effects, At-

- mos. Chem. Phys., 16, 2507–2523, https://doi.org/10.5194/acp-16-2507-2016, 2016.
- Heald, C. L., Ridley, D. A., Kroll, J. H., Barrett, S. R. H., Cady-Pereira, K. E., Alvarado, M. J., and Holmes, C. D.: Contrasting the direct radiative effect and direct radiative forcing of aerosols, Atmos. Chem. Phys., 14, 5513–5527, https://doi.org/10.5194/acp-14-5513-2014, 2014.
- Holben, B. N., Eck, T., Slutsker, I., Smirnov, A., Sinyuk, A., Schafer, J., Giles, D., and Dubovik, O.: AERONET's Version 2.0 quality assurance criteria, Proc. SPIE 6408, Remote Sensing of the Atmosphere and Clouds, 64080Q, https://doi.org/10.1117/12.706524, 2006.
- Huang, X., Ding, K., Liu, J., Wang, Z., Tang, R., Xue, L., Wang, H., Zhang, Q., Tan, Z.-M., Fu, C., Davis, S. J., Andreae, M. O., and Ding, A.: Smoke-weather interaction affects extreme wildfires in diverse coastal regions, Science, 379, 457–461, 2023.
- Jaeglé, L., Quinn, P. K., Bates, T. S., Alexander, B., and Lin, J.-T.: 75
 Global distribution of sea salt aerosols: new constraints from in situ and remote sensing observations, Atmos. Chem. Phys., 11, 3137–3157, https://doi.org/10.5194/acp-11-3137-2011, 2011.
- Jiang, X., Wiedinmyer, C., and Carlton, A. G.: Aerosols from fires: an examination of the effects on ozone photochemistry in the Western United States, Environ. Sci. Technol., 46, 11878–11886, https://doi.org/10.1021/es301541k, 2012.
- Jin, L., Permar, W., Selimovic, V., Ketcherside, D., Yokelson, R. J., Hornbrook, R. S., Apel, E. C., Ku, I.-T., Collett Jr., J. L., Sullivan, A. P., Jaffe, D. A., Pierce, J. R., Fried, A., Coggon, M. M., Gkatzelis, G. I., Warneke, C., Fischer, E. V., and Hu, L.: Constraining emissions of volatile organic compounds from western US wildfires with WE-CAN and FIREX-AQ airborne observations, Atmos. Chem. Phys., 23, 5969–5991, https://doi.org/10.5194/acp-23-5969-2023, 2023.
- Jo, D. S., Park, R. J., Lee, S., Kim, S.-W., and Zhang, X.: A global simulation of brown carbon: implications for photochemistry and direct radiative effect, Atmos. Chem. Phys., 16, 3413–3432, https://doi.org/10.5194/acp-16-3413-2016, 2016.
- Jolly, W. M., Cochrane, M. A., Freeborn, P. H., Holden, Z. A., 95 Brown, T. J., Williamson, G. J., and Bowman, D. M.: Climateinduced variations in global wildfire danger from 1979 to 2013, Nat. Commun., 6, 7537, https://doi.org/10.1038/ncomms8537, 2015.
- June, N., Wang, X., Chen, L. A., Chow, J. C., Watson, J. G., 100 Wang, X., Henderson, B. H., Zheng, Y., and Mao, J.: Spatial and temporal variability of brown carbon in United States: implications for direct radiative effects, Geophys. Res. Lett., 47, e2020GL090332, https://doi.org/10.1029/2020gl090332, 2020.
- Kelesidis, G. A., Neubauer, D., Fan, L. S., Lohmann, U., and Pratsinis, S. E.: Enhanced Light Absorption and Radiative Forcing by Black Carbon Agglomerates, Environ. Sci. Technol., 56, 8610–8618, https://doi.org/10.1021/acs.est.2c00428, 2022.
- Kim, P. S., Jacob, D. J., Fisher, J. A., Travis, K., Yu, K., Zhu, L., Yantosca, R. M., Sulprizio, M. P., Jimenez, J. L., CampuzanoJost, P., Froyd, K. D., Liao, J., Hair, J. W., Fenn, M. A., Butler, C. F., Wagner, N. L., Gordon, T. D., Welti, A., Wennberg, P. O., Crounse, J. D., St. Clair, J. M., Teng, A. P., Millet, D. B., Schwarz, J. P., Markovic, M. Z., and Perring, A. E.:
 Sources, seasonality, and trends of southeast US aerosol: an integrated analysis of surface, aircraft, and satellite observations with the GEOS-Chem chemical transport model, Atmos. Chem.

- Phys., 15, 10411–10433, https://doi.org/10.5194/acp-15-10411-2015, 2015.
- Konovalov, I. B., Golovushkin, N. A., Beekmann, M., and Andreae, M. O.: Insights into the aging of biomass burning aerosol from satellite observations and 3D atmospheric modeling: evolution of

the aerosol optical properties in Siberian wildfire plumes, Atmos. Chem. Phys., 21, 357–392, https://doi.org/10.5194/acp-21-357-2021, 2021a.

- Konovalov, I. B., Golovushkin, N. A., Beekmann, M., Panchenko,
 M. V., and Andreae, M. O.: Inferring the absorption properties of organic aerosol in Siberian biomass burning plumes from remote optical observations, Atmos. Meas. Tech., 14, 6647–6673, https://doi.org/10.5194/amt-14-6647-2021, 2021b.
- Lack, D. A. and Langridge, J. M.: On the attribution of black and brown carbon light absorption using the Ångström exponent, Atmos. Chem. Phys., 13, 10535–10543, https://doi.org/10.5194/acp-13-10535-2013, 2013.
- Laskin, A., Laskin, J., and Nizkorodov, S. A.: Chemistry of atmospheric brown carbon, Chem. Rev., 115, 4335–4382, https://doi.org/10.1021/cr5006167, 2015.
- Li, C., van Donkelaar, A., Hammer, M. S., McDuffie, E. E., Burnett, R. T., Spadaro, J. V., Chatterjee, D., Cohen, A. J., Apte, J. S., Southerland, V. A., Anenberg, S. C., Brauer, M., and Martin, R. V.: Reversal of trends in global fine particulate matter air pol-
- b lution, Nat. Commun., 14, 5349, https://doi.org/10.1038/s41467-023-41086-z, 2023.
- Li, M., Zhang, Q., Kurokawa, J.-I., Woo, J.-H., He, K., Lu, Z., Ohara, T., Song, Y., Streets, D. G., Carmichael, G. R., Cheng, Y., Hong, C., Huo, H., Jiang, X., Kang, S., Liu, F., Su, H.,
- and Zheng, B.: MIX: a mosaic Asian anthropogenic emission inventory under the international collaboration framework of the MICS-Asia and HTAP, Atmos. Chem. Phys., 17, 935–963, https://doi.org/10.5194/acp-17-935-2017, 2017.
- Lin, P., Bluvshtein, N., Rudich, Y., Nizkorodov, S. A., Laskin, J., and Laskin, A.: Molecular Chemistry of Atmospheric Brown Carbon Inferred from a Nationwide Biomass Burning Event, Environ. Sci. Technol., 51, 11561–11570, https://doi.org/10.1021/acs.est.7b02276, 2017.
- Liu, J., Bergin, M., Guo, H., King, L., Kotra, N., Edgerton, E., and Weber, R. J.: Size-resolved measurements of brown carbon in water and methanol extracts and estimates of their contribution to ambient fine-particle light absorption, Atmos. Chem. Phys., 13, 12389–12404, https://doi.org/10.5194/acp-13-12389-2013, 2013.
- 45 Liu, J., Scheuer, E., Dibb, J., Ziemba, L. D., Thornhill, K. L., Anderson, B. E., Wisthaler, A., Mikoviny, T., Devi, J. J., Bergin, M., and Weber, R. J.: Brown Carbon in the Continental Troposphere, Geophys. Res. Lett., 41, 2191–2195, https://doi.org/10.1002/2013GL058976, 2014.
- 50 Marais, E. A. and Wiedinmyer, C.: Air Quality Impact of Diffuse and Inefficient Combustion Emissions in Africa (DICE-Africa), Environ. Sci. Technol., 50, 10739–10745, https://doi.org/10.1021/acs.est.6b02602, 2016.
- National Emissions Inventory (NEI) Data: https://www.epa.gov/air-emissions-inventories/ 2011-national-emissions-inventory-nei-data, last access: 27 May 2011.
 - Nie, D., Chen, M., Wu, Y., Ge, X., Hu, J., Zhang, K., and Ge, P.: Characterization of Fine Particulate Matter and

- Associated Health Burden in Nanjing, International Journal of Environmental Research and Public Health, 15, 602, https://doi.org/10.3390/ijerph15040602, 2018.
- Park, R. J. and Jacobb, D. J.: Sources of carbonaceous aerosols over the United States and implications for natural visibility, J. Geophys. Res., 108, https://doi.org/10.1029/2002jd003190, 2003.
- Prather, M. J., Zhu, X., Flynn, C. M., Strode, S. A., Rodriguez, J. M., Steenrod, S. D., Liu, J., Lamarque, J.-F., Fiore, A. M., Horowitz, L. W., Mao, J., Murray, L. T., Shindell, D. T., and Wofsy, S. C.: Global atmospheric chemistry which air matters, Atmos. Chem. Phys., 17, 9081–9102, 70 https://doi.org/10.5194/acp-17-9081-2017, 2017.
- Pye, H. O. T., Chan, A. W. H., Barkley, M. P., and Seinfeld, J. H.: Global modeling of organic aerosol: the importance of reactive nitrogen (NO_x and NO₃), Atmos. Chem. Phys., 10, 11261–11276, https://doi.org/10.5194/acp-10-11261-2010, 2010.
- Randerson, J. T., van der Werf, G. R., Giglio, L., Collatz, G. J., and Kasibhatla, P. S.: Global Fire Emissions Database, Version 4.1 (GFEDv4), ORNL Distributed Active Archive Center [data set], https://doi.org/10.3334/ornldaac/1293, 2017.
- Saleh, R., Robinson, E. S., Tkacik, D. S., Ahern, A. T., Liu, 80 S., Aiken, A. C., Sullivan, R. C., Presto, A. A., Dubey, M. K., Yokelson, R. J., Donahue, N. M., and Robinson, A. L.: Brownness of organics in aerosols from biomass burning linked to their black carbon content, Nat. Geosci., 7, 647–650, https://doi.org/10.1038/ngeo2220, 2014.
- Schnitzler, E. G., Gerrebos, N. G. A., Carter, T. S., Huang, Y., Heald, C. L., Bertram, A. K., and Abbatt, J. P. D.: Rate of atmospheric brown carbon whitening governed by environmental conditions, P. Natl. Acad. Sci. USA, 119, e2205610119, https://doi.org/10.1073/pnas.2205610119, 2022.
- Selimovic, V., Yokelson, R. J., McMeeking, G. R., and Coefield, S.: Aerosol mass and optical properties, smoke influence on O₃, and high NO₃ production rates in a western US city impacted by wildfires, J. Geophys. Res.-Atmos., 125, e2020JD032791, https://doi.org/10.1029/2020jd032791, 2020.
- Shah, V., Jacob, D. J., Li, K., Silvern, R. F., Zhai, S., Liu, M., Lin, J., and Zhang, Q.: Effect of changing NO_x lifetime on the seasonality and long-term trends of satellite-observed tropospheric NO₂ columns over China, Atmos. Chem. Phys., 20, 1483–1495, https://doi.org/10.5194/acp-20-1483-2020, 2020.
- Shamjad, P. M., Satish, R. V., Thamban, N. M., Rastog, N., and Tripathi, S. N.: Absorbing Refractive Index and Direct Radiative Forcing of Atmospheric Brown Carbon over Gangetic Plain, ACS Earth Space Chem., 2, 31–37, https://doi.org/10.1021/acsearthspacechem.7b00074, 2018.
- Shao, J., Chen, Q., Wang, Y., Lu, X., He, P., Sun, Y., Shah, V., Martin, R. V., Philip, S., Song, S., Zhao, Y., Xie, Z., Zhang, L., and Alexander, B.: Heterogeneous sulfate aerosol formation mechanisms during wintertime Chinese haze events: air quality model assessment using observations of sulfate oxygen isotopes in Beijing, Atmos. Chem. Phys., 19, 6107–6123, https://doi.org/10.5194/acp-19-6107-2019, 2019.
- Srinivas, B., Rastogi, N., Sarin, M. M., Singh, A., and Singh, D.: Mass absorption efficiency of light absorbing organic aerosols from source region of paddy-residue burning emissions in the Indo-Gangetic Plain, Atmos. Environ., 125, 360–370, https://doi.org/10.1016/j.atmosenv.2015.07.017, 2016.

- Sun, J., Zhang, Y., Zhi, G., Hitzenberger, R., Jin, W., Chen, Y., Wang, L., Tian, C., Li, Z., Chen, R., Xiao, W., Cheng, Y., Yang, W., Yao, L., Cao, Y., Huang, D., Qiu, Y., Xu, J., Xia, X., Yang, X., Zhang, X., Zong, Z., Song, Y., and Wu, C.: Brown carbon's emission factors and optical characteristics in household biomass burning: developing a novel algorithm for estimating the contribution of brown carbon, Atmos. Chem. Phys., 21, 2329–2341, https://doi.org/10.5194/acp-21-2329-2021, 2021.
- Thapa, L. H., Ye, X., Hair, J. W., Fenn, M. A., Shingler, T., Kondragunta, S., Ichoku, C., Dominguez, R., Ellison, L., Soja, A. J., Gargulinski, E., Ahmadov, R., James, E., Grell, G. A., Freitas, S. R., Pereira, G., and Saide, P. E.: Heat flux assumptions contribute to overestimation of wildfire smoke injection into the free troposphere, Commun. Earth Environ., 3, 236, https://doi.org/10.1038/s43247-022-00563-x, 2022.
- The International GEOS-Chem User Community: geoschem/geoschem: GEOS-Chem 12.8.2 (12.8.2), Zenodo [code], https://doi.org/10.5281/zenodo.3860693 (last access: 15 February 2025), 2020.
- 20 Thompson, C. R., Wofsy, S. C., Prather, M. J., Newman, P. A., Hanisco, T. F., Ryerson, T. B., Fahey, D. W., Apel, E. C., Brock, C. A., Brune, W. H., Froyd, K., Katich, J. M., Nicely, J. M., Peischl, J., Ray, E., Veres, P. R., Wang, S., Allen, H. M., Asher, E., Bian, H., Blake, D., Bourgeois, I., Budney, J., Bui, T. P., But-
- ler, A., Campuzano-Jost, P., Chang, C., Chin, M., Commane, R.,
 Correa, G., Crounse, J. D., Daube, B., Dibb, J. E., DiGangi, J.
 P., Diskin, G. S., Dollner, M., Elkins, J. W., Fiore, A. M., Flynn,
 C. M., Guo, H., Hall, S. R., Hannun, R. A., Hills, A., Hintsa,
 E. J., Hodzic, A., Hornbrook, R. S., Huey, L. G., Jimenez, J.
- L., Keeling, R. F., Kim, M. J., Kupc, A., Lacey, F., Lait, L. R., Lamarque, J.-F., Liu, J., McKain, K., Meinardi, S., Miller, D. O., Montzka, S. A., Moore, F. L., Morgan, E. J., Murphy, D. M., Murray, L. T., Nault, B. A., Neuman, J. A., Nguyen, L., Gonzalez, Y., Rollins, A., Rosenlof, K., Sargent, M., Schill, G.,
- Schwarz, J. P., Clair, J. M. S., Steenrod, S. D., Stephens, B. B., Strahan, S. E., Strode, S. A., Sweeney, C., Thames, A. B., Ullmann, K., Wagner, N., Weber, R., Weinzierl, B., Wennberg, P. O., Williamson, C. J., Wolfe, G. M., and Zeng, L.: The NASA Atmospheric Tomography (ATom) Mission: Imaging the Chemistry
- of the Global Atmosphere, B. Am. Meteorol. Soc., 103, E761–E790, https://doi.org/10.1175/bams-d-20-0315.1, 2022.
- Val Martin, M., Logan, J. A., Kahn, R. A., Leung, F.-Y., Nelson,D. L., and Diner, D. J.: Smoke injection heights from fires inNorth America: analysis of 5 years of satellite observations, At-
- mos. Chem. Phys., 10, 1491–1510, https://doi.org/10.5194/acp-10-1491-2010, 2010.
 - van der Werf, G. R., Randerson, J. T., Giglio, L., van Leeuwen, T. T., Chen, Y., Rogers, B. M., Mu, M., van Marle, M. J. E., Morton, D. C., Collatz, G. J., Yokelson, R. J., and Kasibhatla, P. S.: Global
- fire emissions estimates during 1997–2016, Earth Syst. Sci. Data, 9, 697–720, https://doi.org/10.5194/essd-9-697-2017, 2017.
- Wang, X., Heald, C. L., Ridley, D. A., Schwarz, J. P., Spackman, J. R., Perring, A. E., Coe, H., Liu, D., and Clarke, A. D.: Exploiting simultaneous observational constraints on mass and absorp-
- tion to estimate the global direct radiative forcing of black carbon and brown carbon, Atmos. Chem. Phys., 14, 10989–11010, https://doi.org/10.5194/acp-14-10989-2014, 2014.
 - Wang, X., Heald, C. L., Liu, J., Weber, R. J., Campuzano-Jost, P., Jimenez, J. L., Schwarz, J. P., and Perring, A. E.: Exploring the

- observational constraints on the simulation of brown carbon, Atmos. Chem. Phys., 18, 635–653, https://doi.org/10.5194/acp-18-635-2018, 2018.
- Washenfelder, R. A., Attwood, A. R., Brock, C. A., Guo, H., Xu, L., Weber, R. J., Ng, N. L., Allen, H. M., Ayres, B. R., Baumann, K., Cohen, R. C., Draper, D. C., Duffey, K. C., Edgerton, E., Fry, J. L., Hu, W. W., Jimenez, J. L., Palm, B. B., Romer, P., Stone, E. A., Wooldridge, P. J., and Brown, S. S.: Biomass burning dominates brown carbon absorption in the rural southeastern United States, Geophys. Res. Lett., 42, 653–664, https://doi.org/10.1002/2014gl062444, 2015.
- Wu, C., Wang, G., Li, J., Li, J., Cao, C., Ge, S., Xie, Y., Chen, J., Li, X., Xue, G., Wang, X., Zhao, Z., and Cao, F.: The characteristics of atmospheric brown carbon in Xi'an, inland China: sources, size distributions and optical properties, Atmos. Chem. Phys., 20, 2017–2030, https://doi.org/10.5194/acp-20-2017-2020, 2020.
- Wu, G., Ram, K., Fu, P., Wang, W., Zhang, Y., Liu, X., Stone, E. A., Pradhan, B. B., Dangol, P. M., Panday, A., Wan, X., Bai, Z. P., Kang, S., Zhang, Q., and Cong, Z.: Water-Soluble Brown Carbon in Atmospheric Aerosols from Godavari (Nepal), a Regional Representative of South Asia, Environ. Sci. Technol., 53, 3471–80 3479, https://doi.org/10.1021/acs.est.9b00596, 2019.
- xe_xie; xiexinchun/xxc: simu-brc-new (simu-brc), Zenodo [code], https://doi.org/10.5281/zenodo.17346391, 2025.
- Xie, X., Chen, Y., Nie, D., Liu, Y., Liu, Y., Lei, R., Zhao, X., Li, H., and Ge, X.: Light-absorbing and fluorescent properties of atmospheric brown carbon: A case study in Nanjing, China, Chemosphere, 251, 126350, https://doi.org/10.1016/j.chemosphere.2020.126350, 2020.
- Xu, L., Lin, G., Liu, X., Wu, C., Wu, Y., and Lou, S.: Constraining Light Absorption of Brown Carbon in China and Implications for Aerosol Direct Radiative Effect, Geophys. Res. Lett., 51, e2024GL109861, https://doi.org/10.1029/2024g1109861, 2024.
- Yan, C., Zheng, M., Bosch, C., Andersson, A., Desyaterik, Y., Sullivan, A. P., Collett, J. L., Zhao, B., Wang, S., He, K., and Gustafsson, O.: Important fossil source contribution to brown carbon in Beijing during winter, Sci. Rep., 7, 43182, https://doi.org/10.1038/srep43182, 2017.
- Yue, S., Zhu, J., Chen, S., Xie, Q., Li, W., Li, L., Ren, H., Su, S., Li, P., Ma, H., Fan, Y., Cheng, B., Wu, L., Deng, J., Hu, W., Ren, L., Wei, L., Zhao, W., Tian, Y., Pan, X., Sun, Y., Wang, Z., Wu, F., Liu, C.-Q., Su, H., Penner, J. E., Pöschl, U., Andreae, M. O., Cheng, Y., and Fu, P.: Brown carbon from biomass burning imposes strong circum-Arctic warming, One Earth, 5, 293–304, https://doi.org/10.1016/j.oneear.2022.02.006, 2022.
- Zeng, L., Zhang, A., Wang, Y., Wagner, N. L., Katich, J. M., 105 Schwarz, J. P., Schill, G. P., Brock, C., Froyd, K. D., Murphy, D. M., Williamson, C. J., Kupc, A., Scheuer, E., Dibb, J., and Weber, R. J.: Global Measurements of Brown Carbon and Estimated Direct Radiative Effects, Geophys. Res. Lett., 47, e2020GL088747, https://doi.org/10.1029/2020GL088747, 2020.
- Zhang, A., Wang, Y., Zhang, Y., Weber, R. J., Song, Y., Ke, Z., and Zou, Y.: Modeling the global radiative effect of brown carbon: a potentially larger heating source in the tropical free troposphere than black carbon, Atmos. Chem. Phys., 20, 1901–1920, https://doi.org/10.5194/acp-20-1901-2020, 2020.

115

- Zhang, Y., Forrister, H., Liu, J., Dibb, J., Anderson, B., Schwarz, J. P., Perring, A. E., Jimenez, J. L., Campuzano-Jost, P., Wang, Y., Nenes, A., and Weber, R. J.: Top-of-atmosphere radiative forcing affected by brown carbon in the upper troposphere, Nat. Geosci.,
- 10, 486-489, https://doi.org/10.1038/ngeo2960, 2017.
- Zheng, B., Ciais, P., Chevallier, F., Yang, H., Canadell, J. G., Chen, Y., van der Velde, I. R., Aben, I., Chuvieco, E., Davis, S. J., Deeter, M., Hong, C., Kong, Y., Li, H., Li, H., Lin, X., He, K., and Zhang, Q.: Record-high CO2 emissions from boreal fires in 2021, Science, 379, 912-917, 10 https://doi.org/10.1126/science.ade0805, 2023.



Remarks from the typesetter

Please give an explanation of why this needs to be changed. We have to ask the handling editor for approval. Thanks.

Please confirm citation and corresponding reference list entry.

